


# A model to optimise the selection of marine dual-fuel low-speed diesel engines

Cristofer Hood Marques<sup>1,2</sup>  · Carlos Rodrigues Pereira Belchior<sup>2</sup> · Jean David Job Emmanuel Marie Caprace<sup>2</sup>

Received: 29 November 2016 / Accepted: 30 May 2017 / Published online: 5 June 2017  
© Sociedade Brasileira de Engenharia Naval 2017

**Abstract** This study aimed to address the state of the art of marine diesel engines computer simulation models and the main computer applications. There are simple models based on transfer function or more complex models based on computational fluid dynamics. The models may be either implemented through basic programming languages or simulated through dedicated packages of internal combustion engine simulation. Owing to the recent interest to reduce the gas emission, dual-fuel engines are increasingly being used as primary propulsion in merchant ships. In this context, a simplified model of marine dual-fuel low-speed diesel engine has been developed. Through the normalisation of specific fuel consumption and exhaust gas data, clear trends approachable by polynomial curves or surfaces were revealed. Thus, by using the proposed model and knowing the characteristics of an engine at its nominal maximum continuous rating, it is possible to predict the engine operation in any design point on the engine layout diagram, even at part load. The maximum deviations regarding the two simulated engines did not exceed –3.4%. Summarising, the developed model is a simple and effective tool for optimising the selection of dual-fuel low-speed diesel engines to be applied in ship propulsion systems.

**Keywords** Marine propulsion · Prime mover · Optimisation · Prediction model · Selection

---

✉ Cristofer Hood Marques  
cristoferhood@oceanica.ufrj.br

<sup>1</sup> Federal University of Rio Grande – FURG, Rio Grande, Brazil

<sup>2</sup> Federal University of Rio de Janeiro – COPPE/UFRJ, Rio de Janeiro, Brazil

## 1 Introduction

The earliest engine models were based on ideal (air standard) cycles [1] and are currently the most widely taught in undergraduate courses. Although these were very simplistic, they helped the engineers to understand engine operation. The first of these models is supposed to have been developed in the late 1800s [2].

On the other hand, internal combustion engine simulations itself have been developed and applied since the 1960s. It consists in reproducing mathematically the significant processes and predicting the performance and operation details. In the beginning, the simulations were fairly elementary and limited by both computing capabilities and a lack of knowledge concerning some key sub-models. Nowadays, many of these simulations contain advanced and detailed sub-models about fluid mechanics, heat transfer, friction, combustion and chemical kinetics, being performed by sophisticated computer programs [3].

The earliest works on compression ignition engines are perhaps due to McAulay et al. [4], as well as Krieger and Borman [5]. Their simulations were fairly complete, but a major weakness was the lack of a comprehensive description of the complex diesel engine combustion process.

The development of engine cycle simulations is a challenging task largely because of turbulent and unsteady flow, non-uniform mixture composition, highly exothermic chemical reactions, two or three phase compositions, as well as pollutant species. In addition, the important time scales have a large dynamic range of between 1  $\mu$ s and 1 s, and the important length scales range roughly between 1  $\mu$ m and 1 m.

According to Schulten [6], five main sorts of engine model might be recognised: computational fluid dynamics

(CFD) models, phenomenological multi-dimensional models, crank angle models, mean value models and transfer function models.

Within CFD engine models, which are the most complexes, the volume studied is divided in thousands of volumes or elements, and the basic conservation equations are solved for each volume. Being usually used only for processes occurring inside the cylinder and the ducts of admission and discharge, this modelling provides detailed information and requires powerful computers, besides high computational time. On the other hand, if the cylinder is divided into a smaller number of volumes (in the order of ten) and, additionally to the basic conservation equations, phenomenological equations are solved, a phenomenological multi-dimensional model is obtained.

Crank angle models are also called zero-dimensional (0-D) because these models do not have a strict mathematical dependence on any of the dimensions. It consists in treating each of the various engine elements as a volume control and solving the differential equations in a time step equivalent to one degree of the crankshaft rotation.

Nevertheless, whether an engine model is inserted into a larger system, such as a propulsion system, the variations that occur for each crankshaft angle of rotation are generally not of primary interest. In this case, overall engine operating parameters are the focus and can be obtained by using a mean value engine model (MVEM). This model basically has the same origin of the 0-D, but as its time step is in the order of one crankshaft rotation, the variation of each parameter within the cylinder is replaced by a mean value.

Finally, when there is no interest at all in the internal processes, the engine can be merely represented by functions. This is the so-called transfer function engine model (TFEM), which is the simplest and fastest method.

The models may be implemented through many scientific languages, such as FORTRAN, MATLAB, C# and C++. Some simulation dedicated packages may also be applied, for instance, CORAL, CSMP, ACSL and SIMULINK. Furthermore, dedicated softwares, such as AVL BOOST, GT-POWER and VIRTUAL ENGINE, may be applied for engine 0-D simulations, whilst multi-dimensional simulations may be performed through CONVERGE, KIVA, OPENFOAM and so on [3].

The most used ship engine within shipping is the low-speed diesel engine and factors influencing its selection can be classified into two categories: technical aspects and financial aspects. Noise, vibration, emissions, size, weight and efficiency are only some examples of the former, whilst capital expenditures and operational expenditures summarise the latter. However, criteria designation is a highly difficult problem due to the shortage of detailed information about the performance and particulars of many products.

The maritime industry has faced new realities that are changing marine fuel investment choices. Although vessels have become cleaner, regulators, environmentalists and health officials are still concerned about pollutants near major coastal population centres. Natural gas offers lower local pollution emissions compared to distillate fuels and can significantly reduce local pollutants from vessel operations. Price differences between natural gas and low-sulphur fuel oil suggest that an economic advantage may favour natural gas. In addition, natural gas infrastructure is growing, making it more plausible to feed ships with natural gas [7]. These are some reasons why dual-fuel diesel engines have become an attractive alternative.

Karim [8] states that the term dual-fuel describes compression ignition engines burning simultaneously two entirely different fuels in varying proportions. In gas mode, these two fuels are usually made up of a gaseous fuel, which supplies much of the energy released through combustion, and a second fuel, which is a liquid employed mainly to provide the energy needed for ignition and the remaining fraction of the energy release by the engine. In diesel mode, these engines work as a conventional diesel engine. Thus, this kind of engine holds three types of specific fuel consumption: specific pilot oil consumption (SPOC) and specific gas consumption (SGC), in gas mode, besides specific fuel oil consumption (SFOC), in diesel mode.

Having regard to the scene that has been hereinbefore mentioned, the present study aims to provide the state of the art about marine diesel engine models as well as proposing a simple and fast model to be used in optimisation problems about marine dual-fuel low-speed diesel engines. In order to avoid consulting the catalogue data for every engine every time the iterative process is carried out, engine operational features were normalised and trends were approximated by polynomials.

## 2 State of the art

The main papers that inspired the authors for the present work are summarised below.

Benvenuto et al. [9] presented a simulation model to predict the behaviour of a marine propulsion system in permanent and transient conditions. The engine model was based on equations and tables and it was set up in SIMULINK environment.

Kyrtatos et al. [10] addressed a propulsion plant simulation of a containership to provide the engine performance in different operating conditions. In this case, a low-speed diesel engine was applied and it was approached by 0-D modelling.

Michalski [11] performed an algorithmic method for determining optimum values of propulsion system parameters in cases where hull resistance and service speed of the ship significantly varies during operation. In this case, the engine was modelled simply as a constant specific fuel consumption figure.

Theotokatos [12] simulated the propulsion plant of a merchant ship in permanent and transient conditions to predict the interaction between the ship and its propulsion subsystems. A MVEM was applied to model the low-speed diesel engine and the problem was solved through SIMULINK. One year later, Theotokatos [13] presented a comparison of its results against reference data and validated his model.

Medica et al. [14] carried out a model for computer simulation of marine low-speed diesel engine focused on situations where the turbo charger is under severe conditions. A 0-D model with two-zone combustion was utilised, and the problem was solved in the SIMULINK environment.

Aldous and Smith [15] investigated the optimum speed in two natural gas carriers. One of the vessels was equipped with a medium-speed dual-fuel diesel engine and electric transmission, whilst the other was equipped with a low-speed dual-fuel diesel engine directly driving the propeller. Both engines were simulated using data from catalogues.

Baldi et al. [16] developed a modular simulation model in SIMULINK environment for large medium-speed marine diesel engines. It was combined MVEM and 0-D model in order to keep the specific advantages of each approach.

Theotokatos et al. [17] performed a numerical study of a marine dual-fuel four-stroke engine through a GT-POWER model. An investigation of the engine steady-state performance and exhaust emissions was carried out at the engine discrete operating modes (diesel and dual-fuel).

It is worth to notice that all models mentioned must be calibrated for each single engine, such that they are not suitable for iterative procedures as optimisation, for instance. Only two papers presented optimisation studies: Michalski [11] modelled the engine as a constant specific fuel consumption figure, whilst Aldous and Smith [15] utilised catalogues data without trying different engines. Therefore, none of the studies addressed the optimisation of engine selection. Thus, the contribution of the present work is highlighted, that is, the development of a simple and fast engine model to be used in optimisation problems.

### 3 Methodology

Hereinafter, the main steps to obtain the suitable engines and their operational features are explained. Hence, some algorithms were implemented in MATLAB environment.

Owing to the data availability of the Computerised Engine Application System—Engine Room Dimensioning (CEAS-ERD), only engines provided by MAN Diesel & Turbo and covered by this application were studied [18]. Lower heating value has been taken as 42.7 and 50 MJ/kg for liquid fuel and gaseous fuel, respectively.

Although engine type designation refers to the number of cylinders, stroke/bore ratio, diameter of piston, engine concept, mark number, fuel injection concept and Tier III technology, herein narrow engine configurations are studied. Since all the addressed engines are not equipped with Tier III technology, they are of the same fuel injection concept (GI) and engine concept (ME-C); these appointments are not always repeated. Furthermore, ISO ambient conditions and standard configurations were taken, as well as fuel sulphur content of 3.5% was assumed.

#### 3.1 Determination of suitable engines

The first step on engine selection is to place the specified maximum continuous rating (SMCR) point on the engine layout diagram programme to identify which engines are able to supply the required power and speed. Engine layout diagram is an envelope that defines the area where nominal maximum firing pressure is available for the selection of the SMCR. It is limited by two lines of constant mean effective pressure (MEP), L1–L3 and L2–L4, and by two constant engine speed lines, L1–L2 and L3–L4. Figure 1 illustrates the engine layout diagram of the engine 10S90ME-C9.5-GI, as well as the points SMCR and nominal maximum continuous rating (NMCR), which is the same as L1.

In order to cover the entire capacity of the engines, L1 and L3 correspond to the maximum number of cylinders, whilst L2 and L4 correspond to the minimum of cylinders. Figure 2 shows the layout of the engine programme

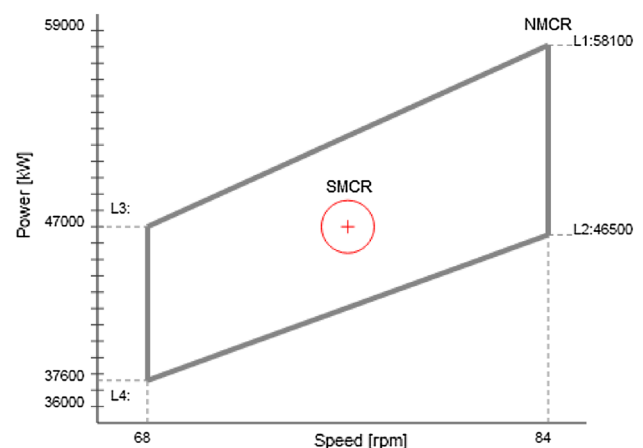


**Fig. 1** Engine layout diagram of the engine 10S90ME-C9.5-GI (adapted from MAN Diesel and Turbo [18])

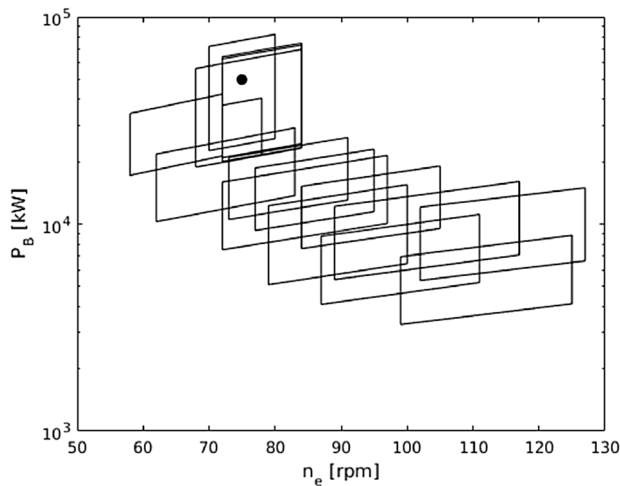


**Fig. 2** Engine layout diagrams of dual-fuel low-speed diesel engines

considered in this study and a SMCR of brake power ( $P_B$ ) equal to 50 MW and engine speed ( $n_e$ ) of 75 rpm.

All necessary information to plot the engine layout diagrams are presented in Table 1. The power per cylinder on the four points ( $P_{Bc,L1}$ ,  $P_{Bc,L2}$ ,  $P_{Bc,L3}$  and  $P_{Bc,L4}$ ), speed limits ( $n_{e,min}$  and  $n_{e,max}$ ) and limitations on the number of cylinders ( $c_{min}$  and  $c_{max}$ ) are considered. As it may be noticed, only engines of type G (green ultra-long stroke) and S (super long stroke) were studied.

### 3.2 Specific fuel consumption at SMCR

Since specific fuel consumption at SMCR depends on its position on the engine layout diagram, the SMCR was

placed on the points L1, L2, L3 and L4 and the operational features of every engine were analysed. Hence, the CEASERD was run four times for every of the sixteen engines totalising sixty-four runs. Considering propeller law with loads between 10 and 100% of SMCR, this application supplies a table with specific fuel consumption in g/kWh, exhaust gas mass flow in kg/s, mixed exhaust gas temperature after turbocharger in °C and a guiding steam production capacity of an exhaust gas boiler at 7.0 bar<sub>a</sub> in kg/h.

Firstly, exhaust gas data were divided by brake power to obtain specific mass flow (SMF), in kg/kWh, and specific temperature (ST), in °C/MW, as stated in Eqs. (1) and (2), respectively. Then, all operational features at SMCR were divided by themselves at NMCR to obtain normalised specific fuel consumptions ( $SFOC_N$ ,  $SGC_N$ ,  $SPOC_N$ ) and normalised specific exhaust gas data ( $SMF_N$  and  $ST_N$ ) regarding NMCR. Equation (3) illustrates this procedure about  $SFOC_N$ .

$$SMF_{ijk} = \frac{MF_{ijk}}{P_{B,ijk}} \cdot 3600 \tag{1}$$

$$ST_{ijk} = \frac{T_{ijk}}{P_{B,ijk}} \cdot 1000 \tag{2}$$

$$SFOC_{N,jk} = \frac{SFOC_{SMCR,jk}}{SFOC_{NMCR,k}} \tag{3}$$

where  $P_B$  is brake power [kW]; the index  $i$  varies between 1 and 19 representing engine loads between 10 and 100% with a step of 5% of the SMCR;  $j$  varies between 1 and 4 representing the SMCR position (L1, L2, L3 and L4) and  $k$  varies between 1 and 16 representing the engines.

**Table 1** Available ME-GI dual-fuel low-speed engines and their particulars to chart the layout diagrams

Engine	$P_{Bc,L1}$ (kW/cyl)	$P_{Bc,L2}$ (kW/cyl)	$P_{Bc,L3}$ (kW/cyl)	$P_{Bc,L4}$ (kW/cyl)	$n_{e,min}$ (rpm)	$n_{e,max}$ (rpm)	$c_{min}$ (-)	$c_{max}$ (-)
G95-9.5	6870	5170	6010	4520	70	80	5	12
G90-10.5	6240	4670	5350	4010	72	84	5	12
S90-10.5	6100	4880	5230	4180	72	84	5	12
S90-9.5	5810	4650	4700	3760	68	84	5	12
G80-9.5	4710	3550	3800	2860	58	72	6	9
S80-9.5	4510	3610	4160	3330	72	78	6	9
G70-9.5	3640	2740	2720	2050	62	83	5	8
S70-8.5	3270	2610	2620	2100	73	91	5	8
S65-8.5	2870	2290	2330	1860	77	95	5	8
G60-9.5	2680	2010	1990	1500	72	97	5	8
S60-8.5	2380	1900	1900	1520	84	105	5	8
G50-9.5	1720	1290	1360	1020	79	100	5	9
S50-9.5	1780	1420	1350	1080	89	117	5	9
S50-8.5	1660	1330	1340	1070	102	127	5	9
G45-9.5	1390	1045	1090	820	87	111	5	8
G40-9.5	1100	825	870	655	99	125	5	8

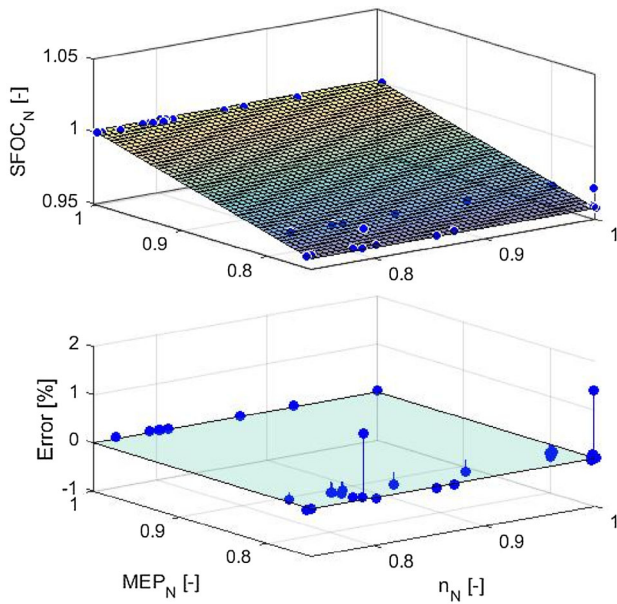


**Fig. 3** Polynomial surface of  $SFOC_N$  and percentage error versus  $MEP_N$  and  $n_N$

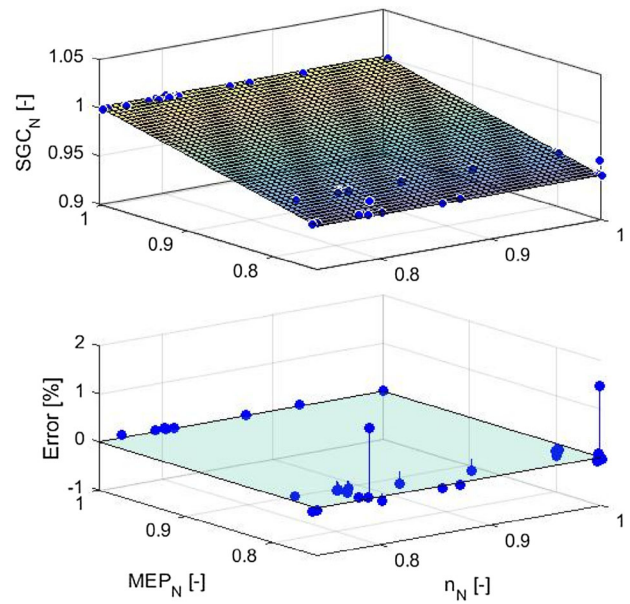


**Fig. 5** Polynomial surface of  $SGC_N$  and percentage error versus  $MEP_N$  and  $n_N$

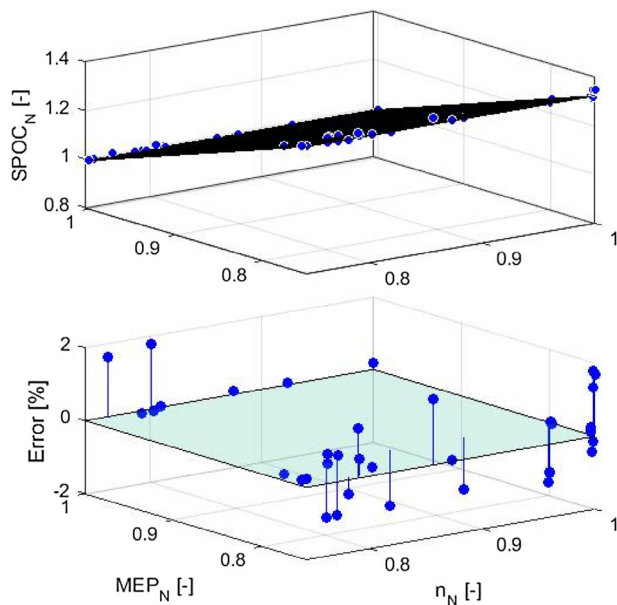


**Fig. 4** Polynomial surface of  $SPOC_N$  and percentage error versus  $MEP_N$  and  $n_N$

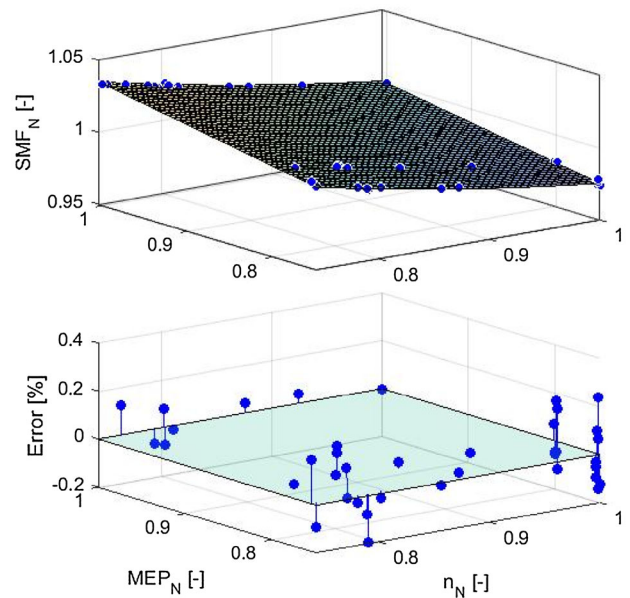


**Fig. 6** Exhaust gas polynomial surface of  $SMF_N$  and percentage error versus  $MEP_N$  and  $n_N$

Polynomial surfaces about normalised specific fuel consumptions and their percentage errors are illustrated in Figs. 3, 4 and 5, whilst normalised exhaust gas polynomial surfaces and percentage errors are shown in Figs. 6 and 7. As illustrated, specific fuel consumptions vary almost linearly with respect to normalised mean effective pressure ( $MEP_N$ ) and are practically not influenced by normalised speed ( $n_N$ ), hence they could be approached with plans. In

contrast, exhaust gas features vary with respect to both  $MEP_N$  and  $n_N$ , such that plans are not the best approach. Even though specific fuel consumptions differ in gas and diesel modes, exhaust gas features are quite similar, such that only one trend of  $SMF_N$  and  $ST_N$  are shown herein. Moreover, it is important to notice that either engines of type G or S did not present substantial differences, such that they were analysed together.

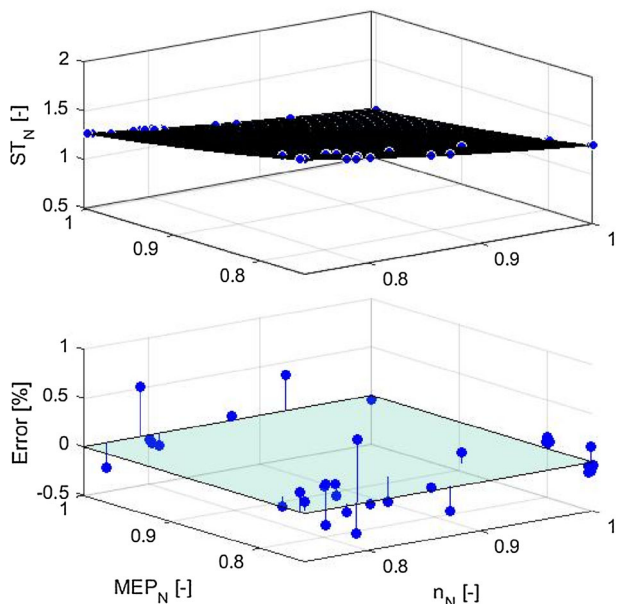


**Fig. 7** Exhaust gas polynomial surface of  $ST_N$  and percentage error versus  $MEP_N$  and  $n_N$

Figure 3 shows specific fuel oil consumption at SMCR normalised with respect to NMCR ( $SFOC_N$ ) and the percentage errors about the fitted plan surface. It draws attention to the fact that the two largest deviations are around 1.4%, whilst all others do not even reach 0.3%. This is due to the engine G40ME-C9.5-GI, which is the only standard fitted with conventional turbocharger instead of high-efficiency turbocharger. On the other hand, the error regarding  $SPOC_N$  peaks at 1.8%, and its average is comparably higher, as illustrated in Fig. 4. Just as the  $SFOC_N$ , Fig. 5 shows that  $SGC_N$  presents only two increased deviations not above 1.5% and the others do not reach 0.3%, which is also due to the engine G40ME-C9.5-GI.

Figure 6 shows specific mass flow of exhaust gas at SMCR normalised with respect to NMCR ( $SMF_N$ ) and the percentage errors about the fitted surface. In this case, only minor deviations are noticed, peaking at about 0.2%. Similarly, the largest deviation regarding  $ST_N$  is under 0.7%, as illustrated in Fig. 7.

### 3.3 Specific fuel consumption at part load

In this case, after obtaining specific operational features, all of them in different engine loads were divided by themselves at SMCR to obtain the normalised specific fuel consumptions ( $SFOC_S$ ,  $SGC_S$ ,  $SPOC_S$ ) and the normalised specific exhaust gas data ( $SMF_S$  and  $ST_S$ ) regarding SMCR. Equation (4) exemplifies this procedure about  $SFOC_S$ .

$$SFOC_{S,ijk} = \frac{SFOC_{ijk}}{SFOC_{SMCR,jk}} \tag{4}$$

where the index  $i$  varies between 1 and 19 representing engine loads between 10 and 100%;  $j$  varies between 1 and 4 representing the SMCR position and  $k$  varies between 1 and 16 representing the engines.

Then, polynomial curves about normalised specific fuel consumptions and their percentage errors, as illustrated in

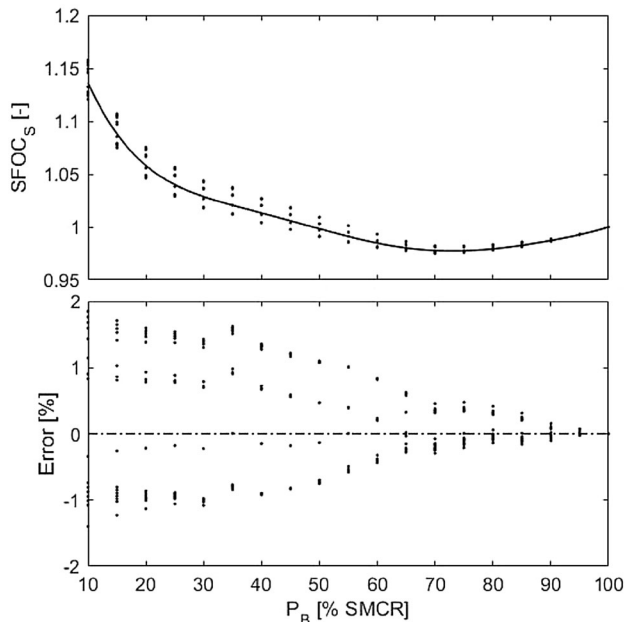


**Fig. 8** Polynomial curve of  $SFOC_S$  and percentage error versus load

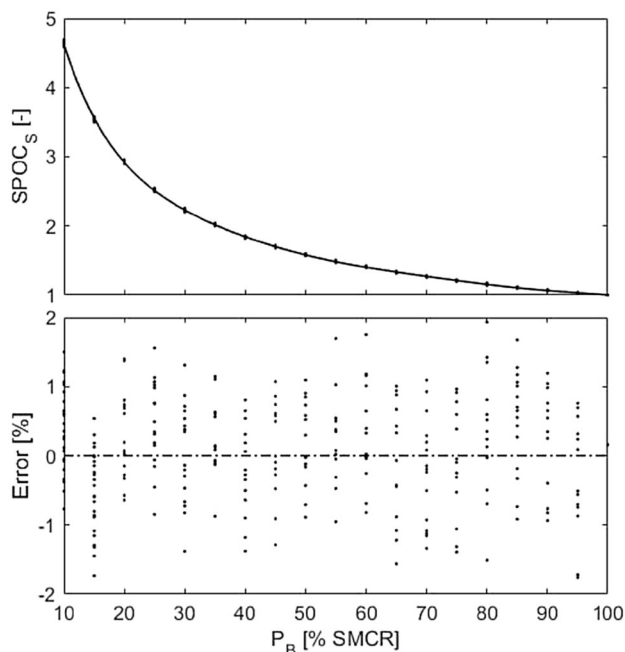


**Fig. 9** Polynomial curve of  $SPOC_S$  and percentage error versus load

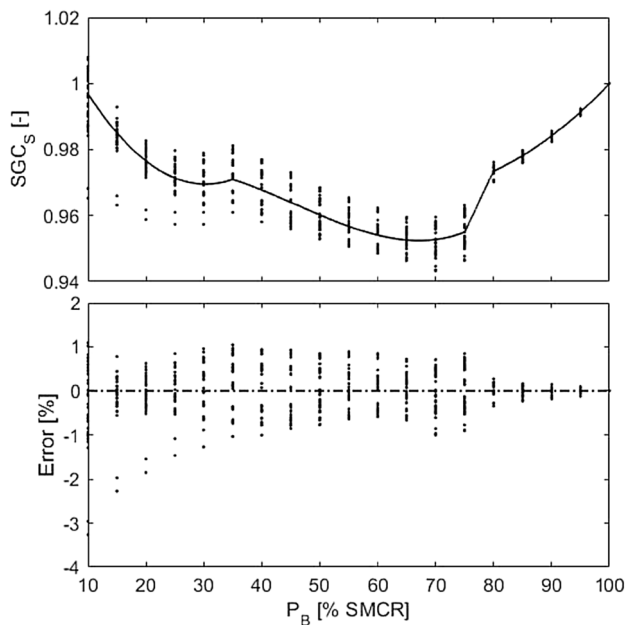


**Fig. 10** Polynomial curve of  $SGC_S$  and percentage error versus load

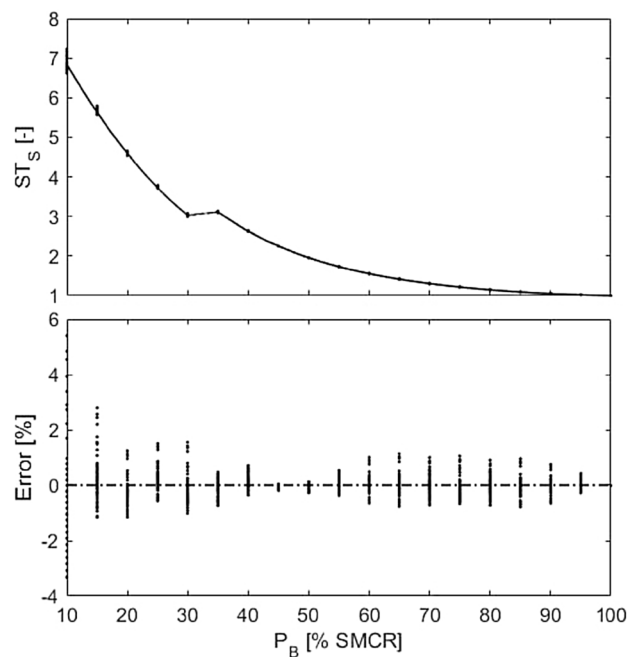


**Fig. 12** Polynomial curve of  $ST_S$  and percentage error versus load

Figs. 8, 9 and 10, were achieved as functions of brake power given in percentage of SMCR (engine load). Meanwhile, normalised exhaust gas polynomial curves and percentage errors are shown in Figs. 11 and 12.

Figure 8 shows that the specific fuel oil consumption normalised with respect to SMCR ( $SFOC_S$ ) presented a minimum value for engine load of 70%. Although there are sixty-four datasets, they are mostly superimposed such that

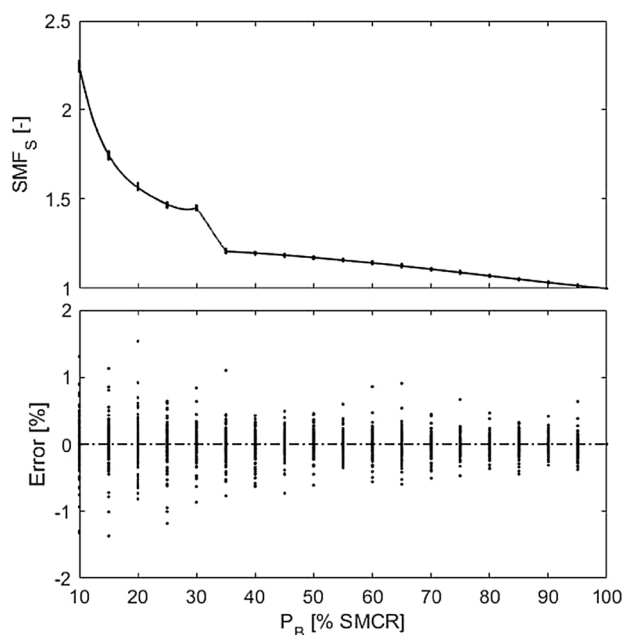


**Fig. 11** Polynomial curve of  $SMF_S$  and percentage error versus load

there are basically four data streams for brake power below 70% of SMCR. Moreover, the mismatches rise as engine load decreases such a way that the greatest is 1.8% for 10% of SMCR. Differently,  $SPOC_S$  grows steadily as load declines and its error is quite dispersed with a maximum about 1.9% for load of 80%, as illustrated in Fig. 9. Meanwhile, four polynomials were needed to approximate more accurately the behaviour of  $SGC_S$  that also presented a global minimum for 70% of SMCR, as shown in Fig. 10. Even so, two data streams stand out and the deviation peaks at  $-3.3\%$ , whilst all the others reach at most  $-1.3\%$ . This is again due to engine G40ME-C9.5-GI, which is the only fitted with conventional turbocharger.

In order to approach specific exhaust gas mass flow and temperature normalised with respect to SMCR ( $SMF_S$  and  $ST_S$ ), three polynomials were applied, as shown in Fig. 11 and 12. In both cases, the widest percentage errors happened for lower loading conditions, such that it was 1.5% for 20% load and 5.4% for 10% load, respectively, about  $SMF_S$  and  $ST_S$ .

### 3.4 Computation procedure

Since polynomials  $SFOC_N$  and  $SFOC_S$  have been achieved and NMCR features are known, specific fuel oil consumption (SFOC) may be evaluated for either engine, SMCR or load, with the following equation:

$$SFOC = SFOC_{NMCR} \cdot SFOC_N \cdot SFOC_S \tag{5}$$

where the polynomial surface  $SFOC_N$  is a function of  $MEP_N$

**Table 2** Specific features at NMCR for gas and diesel mode

Engine	Gas mode				Diesel mode		
	SPOC (g/kWh)	SGC (g/kWh)	SMF (kg/kWh)	ST (°C/MW)	SFOC (g/kWh)	SMF (kg/kWh)	ST (°C/MW)
G95-9.5	5.0	136.7	7.943	2.863	166.0	7.965	2.911
G90-10.5	4.9	135.9	7.942	3.152	165.0	7.966	3.205
S90-10.5	5.0	136.7	7.943	3.224	166.0	7.967	3.279
S90-9.5	5.0	136.7	8.040	3.385	166.0	8.065	3.442
G80-9.5	5.0	136.7	7.745	5.567	166.0	7.762	5.662
S80-9.5	5.0	136.7	8.239	5.814	166.0	8.266	5.913
G70-9.5	5.0	137.5	7.739	7.933	167.0	7.764	8.070
S70-8.5	5.0	139.2	8.243	8.830	169.0	8.271	8.983
S65-8.5	5.0	139.2	8.639	10.06	169.0	8.671	10.24
G60-9.5	5.0	137.5	7.942	10.77	167.0	7.959	10.96
S60-8.5	5.0	139.2	8.641	12.13	169.0	8.660	12.34
G50-9.5	5.0	138.3	7.744	14.92	168.0	7.767	15.18
S50-9.5	5.0	139.2	7.640	14.42	169.0	7.663	14.67
S50-8.5	5.1	140.0	8.651	15.46	170.0	8.675	15.73
G45-9.5	5.1	140.0	7.640	21.22	170.0	7.673	21.58
G40-9.5	5.2	144.1	7.364	29.09	175.0	7.364	29.55

NMCR nominal maximum continuous rating; SFOC specific fuel oil consumption; SGC specific gas consumption; SMF specific mass flow of exhaust gas; SPOC specific pilot oil consumption; ST specific temperature of exhaust gas

and  $n_N$ , as well as the polynomial curve  $SFOC_S$  is a function of engine load in % of SMCR. Furthermore, as it has been asserted hereinbefore,  $MEP_N$  and  $n_N$  are calculated as follows:

$$n_N = \frac{n_{SMCR}}{n_{NMCR}} \tag{6}$$

$$MEP_N = \frac{MEP_{SMCR}}{MEP_{NMCR}} \tag{7}$$

As stated by Woud and Stapersma [19], mean effective pressure may be written as in Eq. (8). Since number of cylinders ( $c$ ), revolutions of crankshaft per complete working cycle ( $r$ ) and cylinder swept volume ( $V_S$ ) are engine constants,  $MEP_N$  could also be written as in Eq. (9). Hence,  $n_N$  and  $MEP_N$  could be calculated with support of Table 1.

$$MEP = \frac{r}{c \cdot V_S} \cdot \frac{P_B}{n_e} \tag{8}$$

$$MEP_N = \frac{P_{SMCR}}{n_{SMCR}} \cdot \frac{n_{NMCR}}{P_{NMCR}} \tag{9}$$

Analogously, SPOC and SGC may be calculated.

Nevertheless, the procedure to evaluate exhaust gas data is a bit different because these were formerly converted into specific variables (divided by brake power). Thus, it is needed to consider the brake power at SMCR ( $P_{SMCR}$ ) and the load fraction ( $f_{SMCR}$ ). Equation (10) illustrates how exhaust gas mass flow (MF) can be calculated.

$$MF = SMF_{NMCR} \cdot SMF_N \cdot SMF_S \cdot P_{SMCR} \cdot f_{SMCR} \tag{10}$$

Analogously, exhaust gas temperature (T) may be calculated.

In order to implement the model, it is thereby necessary to possess only the specific features at NMCR in gas and diesel operational mode for every engine, besides the polynomials. Thus, Table 2 presents SPOC, SGC, SMF and ST for every engine operating in gas mode, as well as SFOC, SMF and ST for diesel mode. Moreover, Table 3 supplies the coefficients ( $p$ ) for every polynomial surface, which was formulated as in Eq. (11), whilst Table 4 is about the polynomial curves, which was formulated as in Eq. (12).

$$z = p_{00} + p_{10}x + p_{01}y + p_{20}x^2 + p_{11}xy + p_{02}y^2, \tag{11}$$

where  $z$  represents  $SPOC_N$ ,  $SGC_N$ ,  $SFOC_N$ ,  $SMF_N$  and  $ST_N$ ,  $x$  is  $n_N$  and  $y$  is  $MEP_N$ .

$$y = p_0 + p_1x + p_2x^2 + p_3x^3 + p_4x^4 + \dots + p_8x^8, \tag{12}$$

where  $y$  represents  $SPOC_S$ ,  $SGC_S$ ,  $SFOC_S$ ,  $SMF_S$  and  $ST_S$ , and  $x$  is engine load. Once every fitted curve was obtained by using centring and scaling transformation to improve the numerical properties of both the polynomial and the fitting algorithm,  $x$  is normalised by the mean ( $\mu$ ) and standard deviation ( $\sigma$ ) given in Table 4 [20].

Since some datasets were approached through more than one polynomial, letters “a”, “b” and “c” given in Table 4 indicate the load range (% of SMCR) where the polynomial is suitable. Regarding  $SGC_N$ , letters indicate ranges from 80 to 100%, 35 to 75% and 10 to 35%, respectively. About



**Table 3** Coefficients of the polynomial surfaces

Coefficients	SPOC <sub>N</sub>	SGC <sub>N</sub>	SFOC <sub>N</sub>	SMF <sub>N</sub>	ST <sub>N</sub>
$p_{00}$	2.297	0.7858	0.8326	1.118	7.320
$p_{10}$	-0.003505	-0.0003174	-0.0004246	-0.3700	-5.328
$p_{01}$	-1.295	0.2143	0.1675	0.1291	-5.883
$p_{20}$	0	0	0	0.1533	1.552
$p_{11}$	0	0	0	-0.03078	1.548
$p_{02}$	0	0	0	0	1.791

Subscript “N” indicates that variable was normalised with respect to NMCR

**Table 4** Coefficients of the polynomial curves

Coeff.	SPOC <sub>S</sub>	SGC <sub>S</sub>			SFOC <sub>S</sub>	SMF <sub>S</sub>		ST <sub>S</sub>	
		a	b	c		a	b	a	b
$p_0 \cdot 10^3$	1485	984.1	956.8	973.6	991.1	1117	1564	1357	4596
$p_1 \cdot 10^3$	-486	9.381	-8.131	-8.866	-37.61	-72.29	-167.1	-443.1	-1349
$p_2 \cdot 10^3$	255.6	1.295	2.578	4.834	15.05	-4.884	73.82	205.3	169.8
$p_3 \cdot 10^3$	-133.9	0	1.244	0	20.71	3.002	-56.51	-69.99	0
$p_4 \cdot 10^3$	-46.64	0	0	0	-1.715	0	34.01	25.05	0
$p_5 \cdot 10^3$	35.38	0	0	0	-10.17	0	0	-4.821	0
$p_6 \cdot 10^3$	49.72	0	0	0	2.932	0	0	0	0
$p_7 \cdot 10^3$	-26.17	0	0	0	0.7298	0	0	0	0
$p_8 \cdot 10^3$	0	0	0	0	-0.1642	0	0	0	0
$\mu$	55.00	90.00	55.00	22.50	55.00	67.50	20.00	67.50	20.00
$\sigma$	27.39	7.082	12.92	8.550	27.39	20.16	7.077	20.16	7.077

Letters “a”, “b” and “c” indicate load range where the polynomial is suitable; subscript “S” indicates that variable was normalised with respect to SMCR;  $\mu$  and  $\sigma$  indicate, respectively, mean and standard deviation of the load range where the polynomial is suitable

SMF<sub>N</sub> and ST<sub>N</sub>, “a” indicates a range from 35 to 100% and “b” from 10 to 30%. In addition, intervals not covered by polynomials could be approximated through linear interpolation.

## 4 Results and discussions

Two engines of intermediary NMCR were simulated and the results were compared against catalogue data (CEAS-ERD). Once the polynomials were reached considering SMCR on L1, L2, L3 and L4, it is necessary to investigate the model accuracy in intermediate points. Therefore, SMCR was additionally placed on the centre of the engine layout diagram (LC), such that the engine 8G70ME-C9.5-GI was examined for 22.3 MW and 73 rpm, as well as the engine 8S70ME-C8.5-GI was examined for 21.1 MW and 82 rpm.

Figures 13 and 14 show fuel consumption polynomials and catalogue data in diesel and gas mode of the engines 8G70ME-C9.5-GI and 8S70ME-C8.5-GI, respectively. It is noticeable that the model is able to predict the behaviour of specific fuel consumptions with only minor mismatches,

even when SMCR is on LC. Comparably, the model is also able to predict the behaviour of exhaust gas for both engines, as illustrated in Figs. 15 and 16. Although exhaust gas mass flow coincides in diesel and gas mode (MF and Mf<sub>g</sub>), temperature in gas mode (T<sub>g</sub>) presents an almost constant drop with respect to diesel mode (T).

Figures 17 and 18 illustrate the percentage errors of the model in diesel mode for the engines 8G70ME-C9.5-GI and 8S70ME-C8.5-GI, respectively. The largest deviations about specific fuel oil consumption (SFOC<sub>e</sub>) and exhaust gas temperature (T<sub>e</sub>) occur for the engine 8G70ME-C9.5-GI when load is 10%. The first is approximately 1.6% when SMCR is either on L2 or L4, and the second is -2.4% when SMCR is on L3, as shown in Fig. 17. Otherwise, 8S70ME-C8.5-GI holds the highest exhaust gas mass flow error (MF<sub>e</sub>), which also come about 10% load, for SMCR on L3, and accounts for -0.6% (Fig. 18).

Finally, Figs. 19 and 20 illustrate the percentage errors of the model in gas mode. The biggest errors about specific gas consumption (SGC<sub>e</sub>), exhaust gas mass flow (Mf<sub>e</sub>) and temperature (T<sub>e</sub>) occur for 10% of SMCR, whilst the greatest deviation regarding specific pilot oil consumption

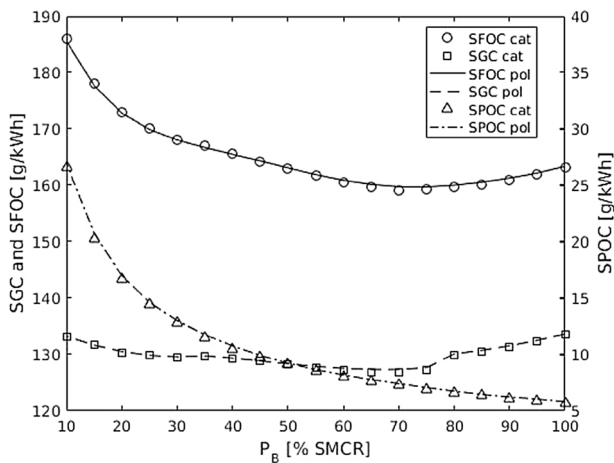


**Fig. 13** Fuel consumption polynomials and catalogue data of the engine 8G70ME-C9.5-GI

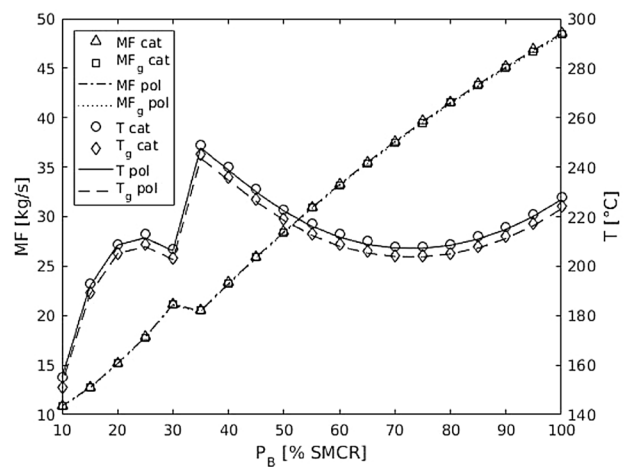


**Fig. 16** Exhaust gas polynomials and catalogue data of the engine 8S70ME-C8.5-GI

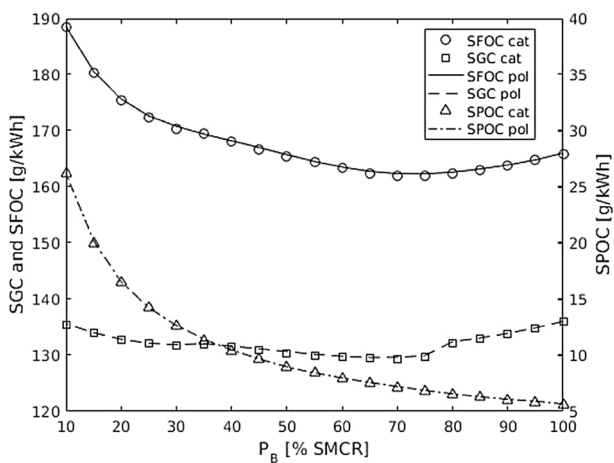


**Fig. 14** Fuel consumption polynomials and catalogue data of the engine 8S70ME-C8.5-GI

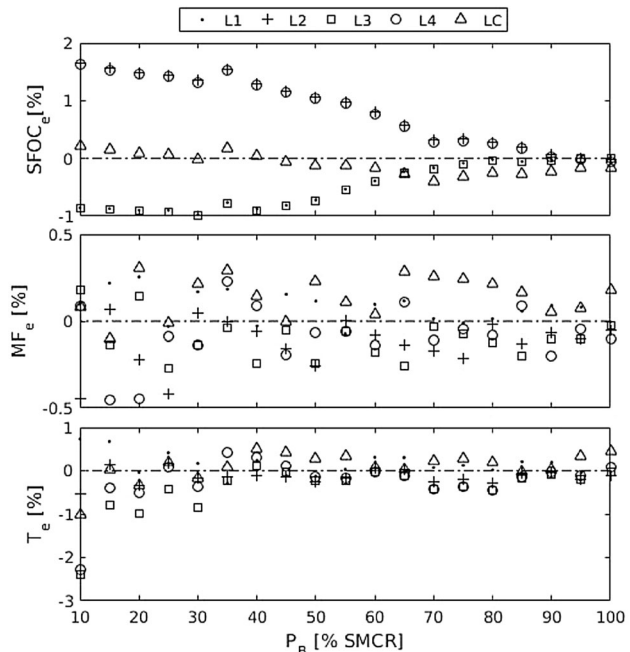


**Fig. 17** Polynomial errors regarding the engine 8G70ME-C9.5-GI in diesel mode

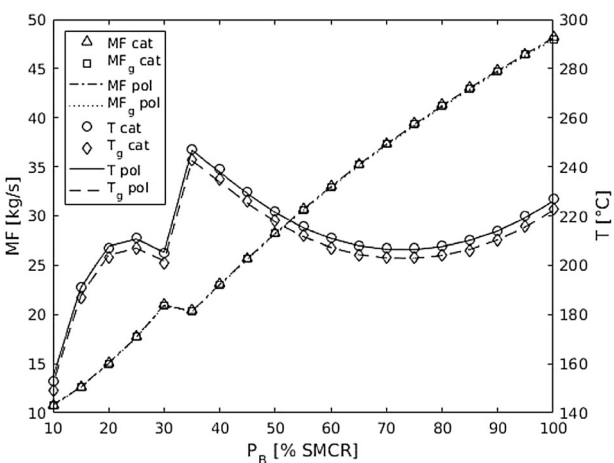


**Fig. 15** Exhaust gas polynomials and catalogue data of the engine 8G70ME-C9.5-GI

(SPOC<sub>e</sub>) takes place when engine load is 95%. The engine 8G70ME-C9.5-GI holds the highest SPOC<sub>e</sub> and T<sub>e</sub>, which are around -2.5 and -3.4%, as well as happen when SMCR is on LC and L3, respectively (Fig. 19). On the other hand, 8S70ME-C8.5-GI holds the highest SGC<sub>e</sub> and MF<sub>e</sub>, which are around -1.1 and 0.6%, as well as happen when SMCR is on L2 and LC, respectively (Fig. 20)

Summarising, the majority of the biggest deviations occurred for brake power equivalent to 10% of SMCR and they did not exceed -3.4% even when SMCR was placed on the centre of the layout diagram.

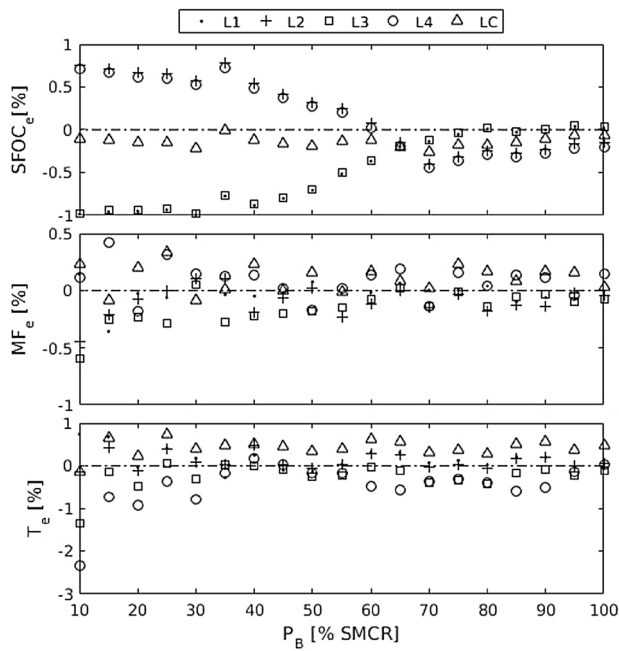


**Fig. 18** Polynomial errors regarding the engine 8S70ME-C8.5-GI in diesel mode

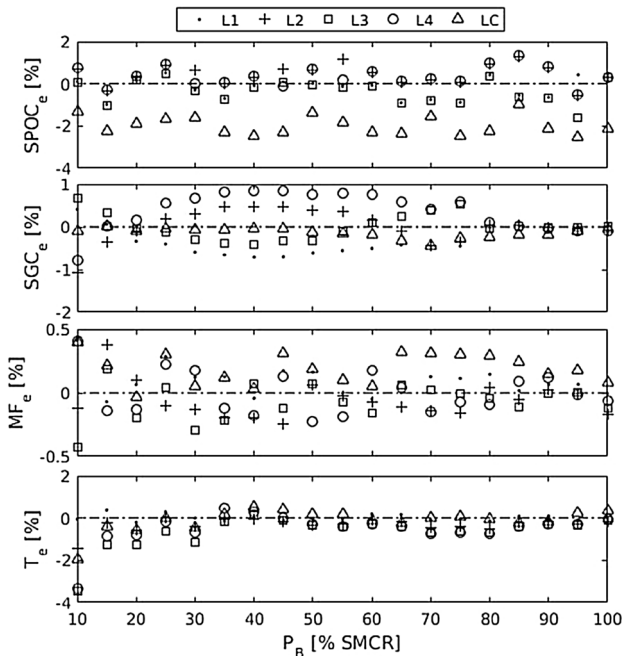


**Fig. 19** Polynomial errors regarding the engine 8G70ME-C9.5-GI in gas mode

## 5 Conclusion

This study has provided the state of the art about models, programming languages and dedicated applications to be used in marine diesel engine simulations. Moreover, a

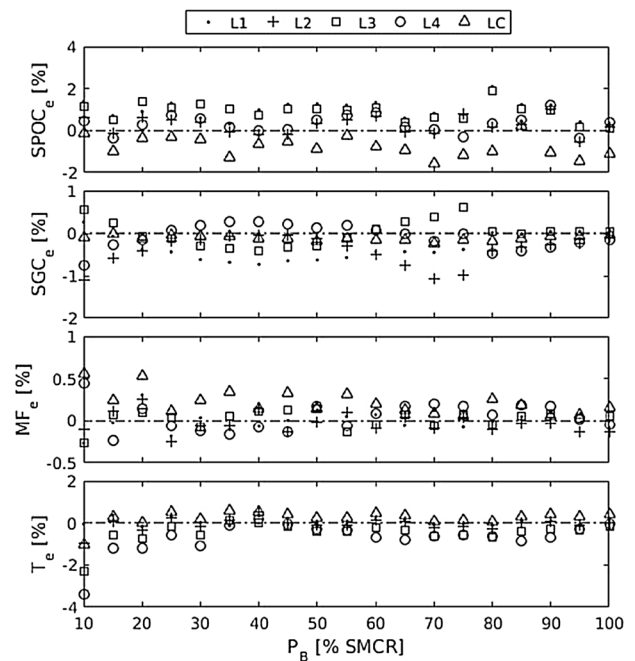


**Fig. 20** Polynomial errors regarding the engine 8S70ME-C8.5-GI in gas mode

simple and fast model to be applied in optimisation problems about selection of marine dual-fuel low-speed diesel engines has been developed. This model was implemented in MATLAB environment, and it is based on normalising engine operational features and approximating their trends with polynomials. Only engines provided by MAN Diesel & Turbo and covered by CEAS-ERD have been studied.

Finally, the results' assessment revealed that the model was not only capable to represent adequately the behaviour of the variables but also presented slight percentage errors. The majority of the biggest deviations regarding the two simulated engines occurred for engine load of 10% and they did not exceed  $-3.4\%$ , even when specified maximum continuous rating was placed on the centre of the layout diagram. Having this figure as quite acceptable, the model may be utilised successfully when one is interested in exhaust gas mass flow and temperature, as well as in specific fuel consumptions.

## References

1. J.B. Heywood, *Internal Combustion Engine Fundamentals* (McGraw-Hill, New York, 1988)
2. D. Clerk, The theory of the gas engine. Minutes Proc. Inst. Civ. Eng. **69**, 220–250 (1882)
3. J.A. Caton, *An Introduction to Thermodynamic Cycle Simulations for Internal Combustion Engines* (Wiley, Chichester, 2016)
4. K.J. Mcaulay, T. Wu, S.K. Chen, G.L. Borman, P.S. Myers, O.A. Uychara, Development and evaluation of the simulation of the

- compression—ignition engine. *Society of Automotive Engineers*, SAE Paper No. 650451, 1965
5. R.B. Krieger, G.L. Borman, The computation of apparent heat release for internal combustion engines. *American Society of Mechanical Engineers*, ASME Paper No. 66WA/DGP- 4, 1966
  6. P.J.M. Schulten, *The interaction between diesel engines, ship and propellers during manoeuvring*. Doctoral Dissertation, Delft University of Technology, Delft, The Netherlands, 2005
  7. H. Thomson, J.J. Corbett, J.J. Winebrake, Natural gas as a marine fuel. *Energy Policy* **87**, 153–167 (2015)
  8. G.A. Karim, *Dual-Fuel Diesel Engines* (CRC Press, Boca Raton, 2015)
  9. G. Benvenuto, G. Carrera, E. Rizzuto, Dynamic Simulation of Marine Propulsion Plants, in *Proceedings of the International Conference on Ship and Marine Research (NAV 94)*, Rome, Italy, 5–7 Oct 1994
  10. N.P. Kyrtatos, P. Theodossopoulos, G. Theotokatos, N. Xiros, Simulation of the overall ship propulsion plant for performance prediction and control. in *Proceedings of the Conference on Advanced Marine Machinery Systems with Low Pollution and High Efficiency*, London, UK, 25–26 March 1999, pp. 103–114
  11. J.P. Michalski, A method for selection of parameters of ship propulsion system fitted with compromise screw propeller. *Pol. Marit. Res.* **14**, 3–9 (2007)
  12. G.P. Theotokatos, A modelling approach for the overall ship propulsion plant simulation, in *Proceedings of the 6th International Conference on System Science and Simulation in Engineering*, Venice, Italy, 21–23 Nov 2007, pp. 80–87
  13. G.P. Theotokatos, Ship propulsion plant transient response investigation using a mean value engine model. *Int. J. Energy* **2**(4), 66–74 (2008)
  14. V. Medica, N. Račić, G. Radica, Performance simulation of marine slow-speed diesel propulsion engine with turbocharger under aggravated conditions. *Strojarstvo* **51**(3), 199–212 (2009)
  15. L. Aldous, T. Smith, Speed optimisation for liquefied natural gas carriers: a techno-economic model, in *Proceedings of the 2nd International Conference on Technologies, Operations, Logistics & Modelling for Low Carbon Shipping*, Newcastle, UK, 11–12 Sept 2012, pp. 1–10
  16. F. Baldi, G. Theotokatos, K. Andersson, Development of a combined mean value—zero dimensional model and application for a large marine four-stroke diesel engine simulation. *Appl. Energy* **154**, 402–415 (2015)
  17. G. Theotokatos, S. Stoumpos, I. Lazakis, G. Livanos, Numerical study of a marine dual-fuel four-stroke engine, in *Proceedings of the 3rd International Conference on Maritime Technology and Engineering (MARTECH)*, Lisbon, Portugal, 4–6 July 2016, pp. 777–783
  18. MAN Diesel & Turbo, *Computerised engine application system—engine room dimensioning (CEAS-ERD)*. <http://marine.man.eu/two-stroke/ceas>, Accessed 01 Dec 2015
  19. H.K. Woud, D. Stapersma, *Design of Propulsion and Electric Power Generation Systems* (IMarEST, London, 2013)
  20. MATHWORKS. *Curve Fitting Toolbox User's Guide*. Version 3.5.3 (R2016a), 2016